J. Non-Newtonian Fluid Mech. 160 (2009) 65–75

Contents lists available at ScienceDirect

Journal of Non-Newtonian Fluid Mechanics

journal homepage: www.elsevier.com/locate/jnnfm

Simulations of complex flow of thixotropic liquids

J.J. Derksen*, Prashant

Chemical & Materials Engineering Department, University of Alberta, Edmonton, Alberta, Canada T6G 2G6

ARTICLE INFO

Article history:
Received 10 February 2009
Received in revised form 23 February 2009
Accepted 25 February 2009

Keywords:
Thixotropy
Simulation
Lattice-Boltzmann
Lid-driven cavity
Mixing tank

ABSTRACT

A procedure for detailed simulations of flow of purely viscous thixotropic liquids is outlined. The local viscosity of the liquid relates to the level of integrity of a network in the liquid. The time-dependence of the liquid's rheology is due to the finite rate with which the network in the liquid builds up or breaks down, the latter due to fluid deformation. This concept has been incorporated in a lattice-Boltzmann discretization of the flow equations coupled to a scalar transport solver with the scalar representing the network integrity. It results in a computationally efficient algorithm that allows for very detailed (three-dimensional and time-dependent) simulations of thixotropic liquid flow in complexly shaped confinements. After verifying the numerical procedure by means of a few benchmark cases, it is applied to study the influence of the Deborah number on the transient behavior as well as the quasi steady-state flow in a mixing tank equipped with a Rushton turbine.

1. Introduction

Many processing and mixing applications involve complex liquids. Examples are specifically abundant in food, pharmaceutical, and related industries; paper and pulp, polymer processing, and also oil sands operations; the latter being the major motivation of the present work. One of the many intriguing phenomena that can occur in complex liquids is the development of a yield stress. Usually the yield stress is the consequence of a network being generated as a result of particle–particle or (macro-) molecular interactions of agents dispersed in a carrier phase. For example, in oil sands processing [1] clay particles get surface activated by (hot) water injection which initiates long range interactions between them. As a result of (ionic) transport limitations, the network is not an instantaneous feature; it takes time to build up, and also to break down as a result of viscous stress and/or deformation in the liquid. In non-homogeneous flows such time-dependent rheology (usually termed thixotropy) is closely linked to the flow dynamics as the (also non-homogeneous) level of network integrity is transported with the flow. It is expected that, from a fluid dynamics point of view, interesting situations occur when the time scales related to the network interfere with characteristic flow time scales.

In the applications that motivate the present work, geometrical complexity of the flows is an essential feature. One should think of flows in agitated tanks, or tube reactors with protrusions (static mixers) and inlet nozzles, or separation devices such as cyclone separators. Also in case of direct simulations of liquid–solid flows with explicit resolution of solid–liquid interfaces geometrical complexity is an issue. In many cases process equipment operates in turbulent or (as is often the case with relatively viscous non-Newtonian liquids) transitional flow regimes. Realistic numerical simulations of such flows require flexibility in setting up computational grids, and above all computational efficiency in order to be able to resolve the flow including its flow structures to a sufficient level of detail. Previous studies [2–4] have shown that the lattice-Boltzmann method [5,6] is a versatile procedure for performing highly resolved computational fluid dynamics of Newtonian fluids. In this paper lattice-Boltzmann simulations of flows of thixotropic liquids in complexly shaped confinements, more specifically mixing tanks, are discussed.

Earlier work on (modeling and simulating) thixotropic liquids has been reviewed by Mewis [7], and at a later stage by Mujumdar et al. [8]. If we (as in the present paper) restrict ourselves to purely viscous liquids (no elasticity effects), Mujumdar et al. show that thixotropy can be effectively implemented in flow solvers by solving an additional scalar transport equation in a parameter characterizing the integrity of the network, and locally coupling this integrity parameter to the apparent viscosity.

A troubling issue regarding simulating non-Newtonian rheology is the steep increase of the number of parameters with increasing complexity of the model characterizing the liquid, and the need to (experimentally and/or computationally) determine their values. For this reason we in the first place choose to limit the number of parameters by adopting a relatively simple thixotropy model, and in the second place choose the thixotropic rheology such that we can easily connect to much simpler Bingham rheology at steady-state conditions.

* Corresponding author.
E-mail addresses: jos@ualberta.ca (J.J. Derksen), pr6@ualberta.ca (Prashant).

0377-0257/$ – see front matter © 2009 Elsevier B.V. All rights reserved.
doi:10.1016/j.jnnfm.2009.02.011

In this paper a procedure for directly simulating thixotropic liquid flow based on a lattice-Boltzmann viscous flow solver is proposed, having in mind the necessity to apply it to turbulent and transitional flows in complexly shaped confinements. In order to build confidence, the procedure is first applied to a few benchmark cases and where possible results are compared to analytical solutions. Subsequently the method is applied to laminar and transitional flows in mixing tanks.

The paper is organized along the lines sketched above. First we briefly discuss thixotropy modeling, and define the model adopted in this paper. Then the translation of the model into a computer algorithm is described. The benchmark cases comprise simple shear flow, plane Poiseuille flow, and lid-driven cavity flow. Finally we demonstrate the feasibility of the numerical approach to simulating mixing tanks containing thixotropic liquids, and conclude this paper.

2. Thixotropy model

The thixotropy model we have adopted is based on early work due to Storey and Merrill [9], and Moore [10], more recently reviewed and applied by Mujumdar et al. [8], and Ferroir et al. [11]. In this purely viscous (i.e. non-elastic) model we keep track of a scalar λ that varies between 0 and 1 and indicates the integrity of the network ($\lambda = 0$: no network; $\lambda = 1$: fully developed network). Its transport equation reads:

$$\frac{\partial \lambda}{\partial t} + u_i \frac{\partial \lambda}{\partial x_i} = -k_1 \dot{\gamma} \lambda + k_2 (1 - \lambda) \tag{1}$$

(summation over repeated indices) with u_i the ith component of the fluid velocity vector, and $\dot{\gamma} = \sqrt{2 d_{ij} d_{ij}}$ a generalized deformation rate; $d_{ij} = 1/2((\partial u_j/\partial x_i) + (\partial u_i/\partial x_j))$ is the rate of strain tensor. The first term on the right hand side of Eq. (1) indicates breakdown of the network due to liquid deformation; the second term is responsible for build-up of the network with a time constant $1/k_2$ associated to it. In the model [11], the apparent viscosity η_a is linked to the network integrity according to:

$$\eta_a = \eta_\infty (1 + \alpha \lambda) \tag{2}$$

In a homogeneous shear field with shear rate $\dot{\gamma}$, the steady-state solution to Eq. (1) reads:

$$\lambda_{ss} = \frac{k_2}{k_1 \dot{\gamma} + k_2} \tag{3}$$

The associated steady-state viscosity is (combine Eqs. (2) and (3)):

$$\eta_{ss} = \eta_\infty \left(1 + \alpha \frac{k_2}{k_1 \dot{\gamma} + k_2} \right) \tag{4}$$

The parameter η_∞ can thus be interpreted as the infinite shear viscosity. The zero-shear viscosity is $\eta_\infty(1 + \alpha)$. A typical representation of the steady-state rheology (Eq. (4)) is given in Fig. 1. As can be seen, it shows some similarity with the rheology of a Bingham liquid, and the dual-viscosity representation often used for mimicking Bingham rheology in viscous flow solvers [12].

In terms of generalized shear, time-independent Bingham rheology reads:

$$\begin{aligned} \tau_{ij} &= 2 \left(\frac{\tau_Y}{\dot{\gamma}} + \eta_B \right) d_{ij} \quad \text{if } |\tau| > \tau_Y \\ d_{ij} &= 0 \qquad\qquad\qquad\quad \text{if } |\tau| \le \tau_Y \end{aligned} \tag{5}$$

with τ_Y the yield stress, $((\tau_Y/\dot{\gamma}) + \eta_B)$ the apparent viscosity, and $|\tau| \equiv \sqrt{(1/2)\tau_{ij}\tau_{ij}}$. In viscous numerical flow solvers (such as the lattice-Boltzmann solver we will be using here), Bingham behavior can be approximated by a two-viscosity model [12]: at very low deformation rates the fluid behaves as a very (though not infinitely) viscous fluid with viscosity η_{B0}. At a critical deformation rate $\dot{\gamma}_{B0}$ the slope in the τ versus $\dot{\gamma}$ curve switches from η_{B0} to η_B (see Fig. 1). This approach introduces an additional (numerical) parameter η_{B0}; the critical deformation rate $\dot{\gamma}_{B0}$ relates to η_{B0} and the physical properties τ_Y and η_B according to $\dot{\gamma}_{B0} = \tau_Y/(\eta_{B0} - \eta_B)$.

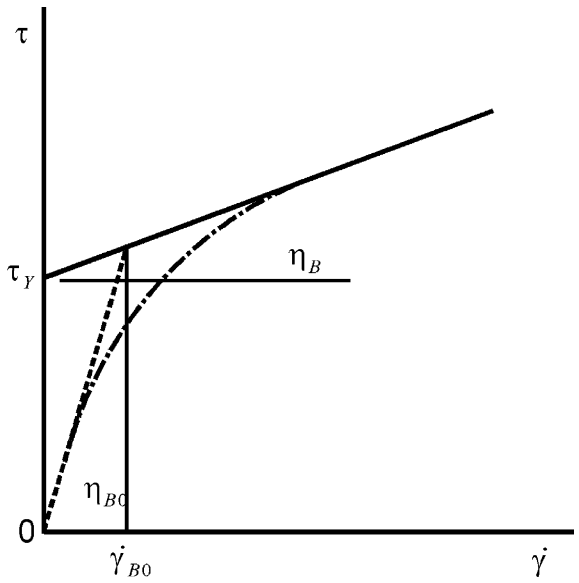

Fig. 1. Steady-state rheology. Solid straight line: Bingham liquid with yield stress τ_Y and slope η_B. Dashed line: in a dual viscosity model the yield stress is mimicked by a very high viscosity (η_{B0}) liquid for low shear. Dash-dotted curve: the steady-state stress–strain behavior of the thixotropic liquid.

The thixotropic liquid as defined by Eqs. (1) and (2) has four parameters: $k_1, k_2, \eta_\infty, \alpha$. For comparing it with time-independent Bingham liquids we note that in steady state it has the same $\dot{\gamma} \to 0$, and $\dot{\gamma} \to \infty$ behavior as the dual-viscosity Bingham model if $\alpha = (\eta_{B0}/\eta_B) - 1$, and if $\eta_\infty \alpha (k_2/k_1) = \tau_Y$. Once we have chosen a network build-up time-scale $1/k_2$ we can set the rest of the four parameters of the thixotropic liquid such as to mimic a liquid that in steady-state exhibits Bingham behavior in the $\dot{\gamma} \to 0$ and $\dot{\gamma} \to \infty$ asymptotes: $k_1 = \eta_B \alpha (k_2/\tau_Y)$, $\eta_\infty = \eta_B$, $\alpha = (\eta_{B0}/\eta_B) - 1$.

3. Flow solver and scalar transport modeling

The lattice-Boltzmann method (LBM) is a nowadays well-established way to numerically solve the incompressible Navier–Stokes equations. The method originates from the lattice-gas automaton concept as conceived by Frisch et al. in 1986 [13]. Lattice gases and lattice-Boltzmann fluids can be viewed as particles moving over a regular lattice, and interacting with one another at lattice sites. These interactions (collisions) give rise to viscous behavior of the fluid, just as colliding/interacting molecules do in real fluids. Since 1987 particle-based methods for mimicking fluid flow have evolved strongly, as can be witnessed from review articles and text books [4–6,14].

The main reasons for employing the LBM for fluid flow simulations are its computational efficiency and its inherent parallelism, both not being hampered by geometrical complexity. More recently LBM has been applied to non-Newtonian fluid mechanics [15–17]. For an in-depth description of the LBM we refer to the excellent monograph due to Succi [6].

In this paper the LBM formulation of Somers [18] has been employed which falls in the category of three-dimensional, 18 speed (D3Q18) models. Its grid is uniform and cubic. Planar, no-slip walls naturally follow when applying the bounce-back condition. For non-planar and/or moving walls (that we have in case we are

simulating the flow in a mixing tank with a revolving impeller) an adaptive force field technique (a.k.a. immersed boundary method) has been used [2,19]. We have employed and validated this method extensively in previous studies involving (turbulent) flow in process equipment (e.g. [2,20]).

For incorporating thixotropy, the viscosity needs to be made dependent on the local value of the network parameter λ (Eq. (2)), and (more importantly) the transport equation for the network parameter (Eq. (1)) needs to be solved. Solving scalar transport equations in a LBM context is an option (see e.g. [21]). It is, however, a relatively expensive approach in terms of computer memory usage: in order to solve for a single scalar we need to allocate as much memory as for solving the Navier–Stokes equations (i.e. 18 real values per lattice node in an 18 speed LBM). Instead we solve Eq. (1) with an explicit finite volume discretization on the same (uniform and cubic) grid as the LBM. This way only two real values per lattice node need to be stored. An additional advantage of employing a finite volume formulation is the availability of methods for suppressing numerical diffusion. This is particularly important in the present application since Eq. (1) does not have a molecular or turbulent diffusion term; in order to correctly solve Eq. (1) we cannot afford to have significant numerical diffusion. As in previous works [3,22], TVD discretization with the Superbee flux limiter for the convective fluxes [23] was employed. We step in time according to an Euler explicit scheme.

The presence of a source term (i.e. the right-hand side) in Eq. (1), combined with the explicit nature of the time stepping sometimes gives rise to unstable behavior. This behavior can be effectively countered by treating the right-hand side semi-implicitly, i.e. by evaluating it in terms of λ at the new time level. In that case the discrete version of Eq. (1) is schematically written as

$$\frac{\lambda^{(n+1)}-\lambda^{(n)}}{\Delta t}+\left(u_i\frac{\partial\lambda}{\partial x_i}\right)^{(n)}=-k_1\dot{\gamma}^{(n)}\lambda^{(n+1)}+k_2(1-\lambda^{(n+1)}) \qquad (6)$$

with the upper index indicating the (discrete) time level. Eq. (6) can be written as an explicit expression in $\lambda^{(n+1)}$ since the right-hand side does not contain spatial derivatives. When discussing the simple-shear benchmark, the results with explicit and implicit treatment of the source term will be compared, and shown to have insignificant differences.

4. Benchmarks

In order to check our numerical approach, a few benchmark cases have been considered: simple shear flow, plane Poiseuille flow, and the flow in a lid driven cavity. In all three benchmarks first the (low Reynolds number) flow of Newtonian liquid with viscosity η_∞ is simulated until it is fully developed. Then we switch on the thixotropic rheology and we monitor the temporal and spatial evolution of the network parameter λ and of the velocity fields as a result of this. This procedure is followed since it largely allows us to isolate the transient effects due to thixotropy from those related to start-up behavior of the flows. For simple shear and Poiseuille flow we can compare the transient numerical results with (semi-) analytical solutions. The lid-driven cavity case illustrates how a slightly more complex flow responds to thixotropy. Steady lid-driven cavity flow also allows for comparing our Bingham-like liquids with simulations from the literature [24,25].

4.1. Simple shear flow

We generate a simple shear flow in a two-dimensional domain by moving two parallel plates in opposite direction. Initially the network parameter λ is set to zero and the liquid in between the plates is Newtonian with viscosity η_∞. Once this Newtonian simple shear flow has fully developed we start (at $t=t_0$) solving the transport equation in λ (Eq. (1)) and applying the viscosity rule (Eq. (2)). We keep track of the shear stress by monitoring the force required to move the plates.

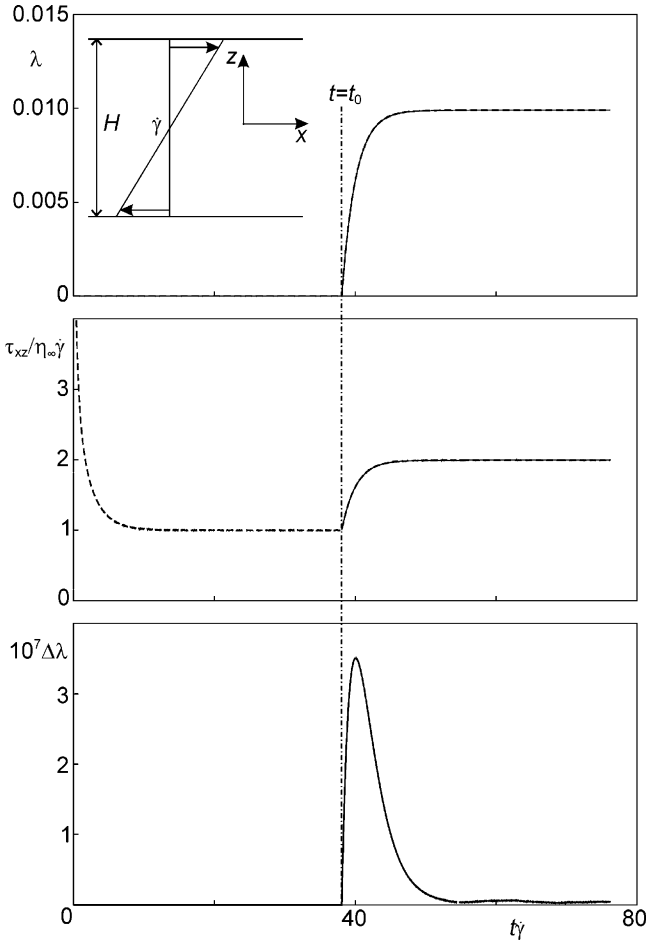

Fig. 2. Time response of a simple shear flow with constant shear rate $\dot{\gamma}$ when switching from Newtonian rheology with dynamic viscosity η_∞ to thixotropic rheology. Top panel: network parameter λ; middle panel: shear stress at the plates; bottom panel $\Delta\lambda\equiv\lambda_{expl}-\lambda_{impl}$. Solid curves: analytical solution; dashed curves: simulations. The flow case shown here has Re = 48, $k_2=5\cdot10^{-3}\dot{\gamma}$, $k_1=0.5$, $\alpha=100$.

In this case of homogeneous shear, the network parameter is homogeneous as well, and Eq. (1) reduces to a linear, ordinary differential equation: $d\lambda/dt=-k_1\dot{\gamma}\lambda+k_2(1-\lambda)$ with solution

$$\lambda=\frac{k_2\{1-\exp[-(k_1\dot{\gamma}+k_2)(t-t_0)]\}}{k_2+k_1\dot{\gamma}} \qquad (7)$$

if $\lambda=0$ at $t=t_0$. As a result, the shear stress responds as $\tau_{zx}=\eta\dot{\gamma}=\eta_\infty[1+\alpha\lambda(t)]\dot{\gamma}$, with $\lambda(t)$ according to Eq. (7).

Typical results are presented in Fig. 2. This specific flow system is fully defined by the following dimensionless numbers: a Reynolds number (here chosen as $Re=\rho\dot{\gamma}H^2/\eta_\infty$ with H the spacing between the two moving plates), k_1, $k_2/\dot{\gamma}$, and α. The figure shows the start-up of the Newtonian flow with liquid being accelerated from zero velocity giving rise to an initially high shear stress on the plates. At $t=t_0$ (when the Newtonian system is fully developed) the thixotropic rheology is switched on which results in an immediate increase in the network parameter λ and (as a consequence) elevated viscosity and shear stress. The simulated results of this transient behavior are in excellent agreement with the analytical solution. In the bottom panel of Fig. 2 we show to what extent the numerical solutions obtained with an implicit treatment of the right hand side of the scalar transport equation differ from those

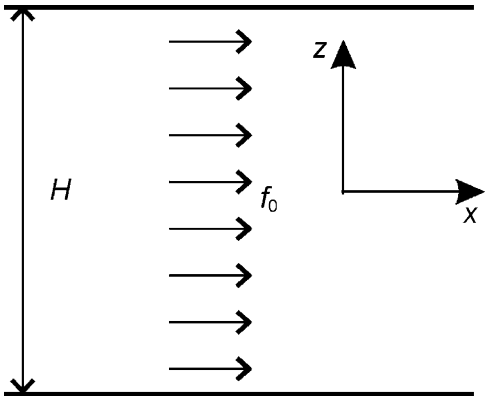

Fig. 3. Planar Poiseuille flow definition.

with an explicit right hand side. There clearly is a systematic effect. It is, however, very minor and only one to two orders of magnitude larger than the accuracy with which numbers are represented in the computer code.

4.2. Plane Poiseuille flow

Compared to simple shear, plane Poiseuille flow is a slightly more complex benchmark. We now have a flow between two fixed parallel plates at mutual distance H driven by a body force (force per unit volume) f_0 in the wall-parallel direction (see Fig. 3 for a definition of the flow and its coordinate system). The body force results in a linear shear stress profile in the liquid: $\tau_{zx} = -f_0 z$. In zero-inertia flow this directly translates in a shear rate $\dot{\gamma} = |(-f_0 z)/(\eta_a(z,t))|$. Since $\eta_a = \eta_\infty(1+\alpha\lambda)$, and since the system is homogeneous in x-direction the transport equation in the network parameter (Eq. (2)) can be written as

$$\frac{\partial \lambda}{\partial t} = -k_1 \lambda \frac{f_0 |z|}{\eta_\infty (1+\alpha\lambda)} + k_2(1-\lambda) \tag{8}$$

In the center of the channel ($z=0$), Eq. (8) implies that λ depends on time according to an exponential function with time constant $1/k_2$. In order to compare the implications of Eq. (8) for the way the network parameter and the velocity field depend on space (z) and time, Eq. (8) was integrated numerically (with a fourth-order Runge–Kutta scheme) for z in the range $-H/2 < z < H/2$. This provides us with a representation of $\lambda(z,t)$ that subsequently is used to determine $\eta_a(z,t)$ (with help of Eq. (2)) and integrate the velocity profile from the notion that $\partial u_x/\partial z = -(f_0 z/\eta_a)$ with $u_x = 0$ at $z = \pm(H/2)$. The results of this semi-analytical exercise can be directly compared with out numerical simulations.

In the simulations we again start from a zero flow field of Newtonian liquid. Once that flow has fully developed (to a parabolic velocity profile in this case) the thixotropic rheology is switched on and we monitor the development of the network and associated apparent viscosity and velocity field. As the velocity scale we take the centerline velocity of the Newtonian liquid: $u_0 = (1/8)(f_0/\eta_\infty)H^2$; the Reynolds number has been defined as $\mathrm{Re} = \rho u_0 H/\eta_\infty$. The results in Fig. 4 show very good agreement of the simulations and the semi-analytical solution. The time scales over which the flow switches from the Newtonian steady state to the non-Newtonian steady state, as well as the profiles of λ and u_x are well represented by the simulations. We see the development of the λ-profile in time: starting from zero λ increases quickest in the center of the channel where there is no deformation. Roughly at $t = 50(H/u_0) = 2.5/k_2$ after switching on the thixotropic rheology the λ profile is close to steady. In the same time range the velocity profile has adapted itself to the new rheology; it has evolved from parabolic to more plug-flow like.

The assumption of zero-inertia as inferred to obtain the semi-analytical solution appears critical. In the right panel of Fig. 4 we compare (at a single moment in time) the semi-analytical solution with simulation results at different Reynolds numbers. The trend is that the agreement clearly benefits from reducing the Reynolds number in the simulations. The results with $\mathrm{Re} < 1$ can hardly be distinguished and are close to the semi-analytical solution.

4.3. Lid-driven cavity flow

The geometry of two-dimensional lid-driven cavity (LDC) flow is given in Fig. 5. The choice for benchmarking our computational approach with LDC flow was partly instigated by simulations of LDC flow of Bingham liquids [24,25]. The results in these papers show clear effects of the liquid's rheology on easily observable quantities such as the location of the vortex center. For Bingham liquids two dimensionless numbers define the flow system: the Reynolds number $\mathrm{Re} = \rho u_0 H/\eta_B$, and a Bingham number $\mathrm{Bn} = \tau_Y H/\eta_B u_0$. For the LDC simulations with thixotropic liquids we apply definitions of dimensionless numbers based on the liquid's asymptotic, steady-state analogy with Bingham liquids (see Section 2). In this analogy, the yield stress relates to thixotropy parameters according to $\tau_Y = \eta_\infty \alpha(k_2/k_1)$, so that the (pseudo) Bingham number becomes $\mathrm{Bn} = \alpha(k_2/k_1)(H/u_0)$. We define the Reynolds number as $\mathrm{Re} = \rho u_0 H/\eta_\infty$. In addition to Re and Bn, a third dimensionless number is the liquid time scale divided by the flow time scale: the Deborah number $\mathrm{Db} = u_0/Hk_2$. It should be noted that having a Deborah number does not imply having viscoelastic effects; in this paper Db purely denotes a ratio of time scales. A fourth dimensionless number is the ratio between the zero-shear and infinite-shear

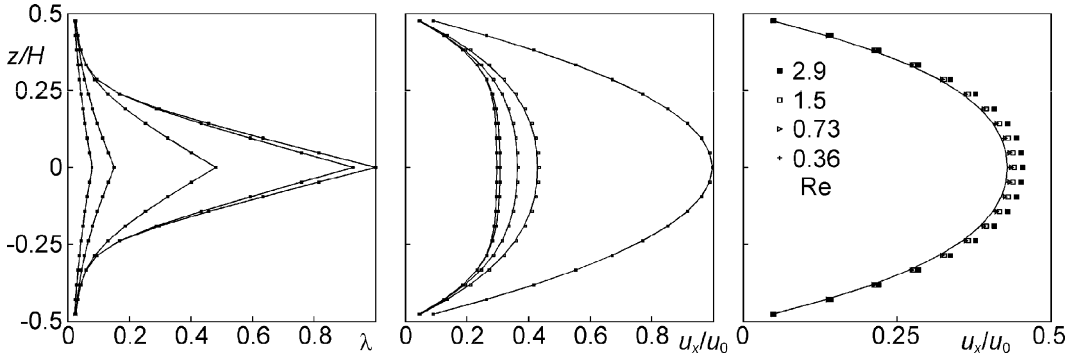

Fig. 4. Profiles of the network parameter λ and velocity in plane channel flow. Drawn curves: semi-analytical solutions; symbols: simulations. Left: λ profiles at various moments ($tu_0/H = 1.6$, 3.3, 13, 52, and 210; λ *increases* with time) after switching on thixotropic rheology. Middle: velocity profiles ($tu_0/H = 0$, 1.6, 3.3, 13, and 52; velocity *decreases* with time). Right: velocity profiles at $tu_0/H = 1.6$ for four different Reynolds numbers. The left and middle panel have $\mathrm{Re} = 0.73$. Furthermore: $k_2 = 5 \times 10^{-2} u_0/H$, $k_1 = 1.0$, α=40.

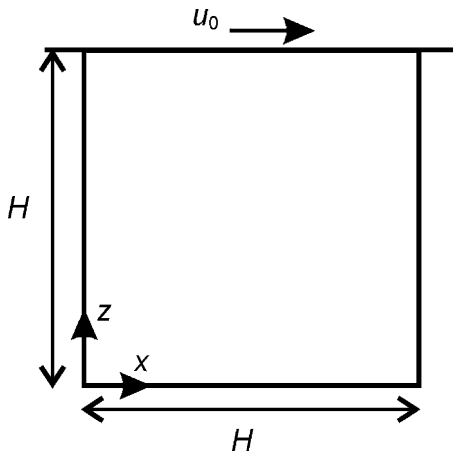

Fig. 5. Definition of the LDC geometry and coordinate system.

viscosity: $\alpha + 1$. In order to focus on the liquid rheology (and not on inertial flow effects) we set the Reynolds number to a fixed, low value: Re = 0.5 throughout the LDC simulations.

The LDC simulations are set up as follows: the default grid consists of $81 \times 1 \times 81$ (xyz) cells. There are no-slip conditions at the four planar walls, and periodic conditions in the third (y) direction (making the simulation effectively two-dimensional). Starting from a zero flow field, the lid is set to move with velocity u_0. Initially the liquid is Newtonian with viscosity η_∞. Once the flow of Newtonian liquid is fully developed the thixotropic rheology is switched on. We then monitor the location of the vortex center, and the force required to move the plate as a function of time. The vortex center is determined by calculating the stream function ψ through integration of the velocity field ($u_x = \partial\psi/\partial z$, $u_z = -(\partial\psi/\partial x)$) and subsequently finding the location of its minimum. Through interpolation we can do that with sub-lattice level accuracy (the accuracy approximately is $0.1\Delta \approx 10^{-3} H$ with Δ the lattice spacing). The force to move the lid follows from the momentum added to the liquid to maintain the no-slip condition at the lid.

For a typical situation, the initial (Newtonian) flow and the ultimate (i.e. steady) LDC flow of thixotropic liquid are shown in Fig. 6 in terms of velocity vectors. The differences are apparent. The thixotropic flow has its vortex center much closer to the moving wall. As compared to the Newtonian flow, the shear thinning behavior of the thixotropic liquid makes the regions away from the

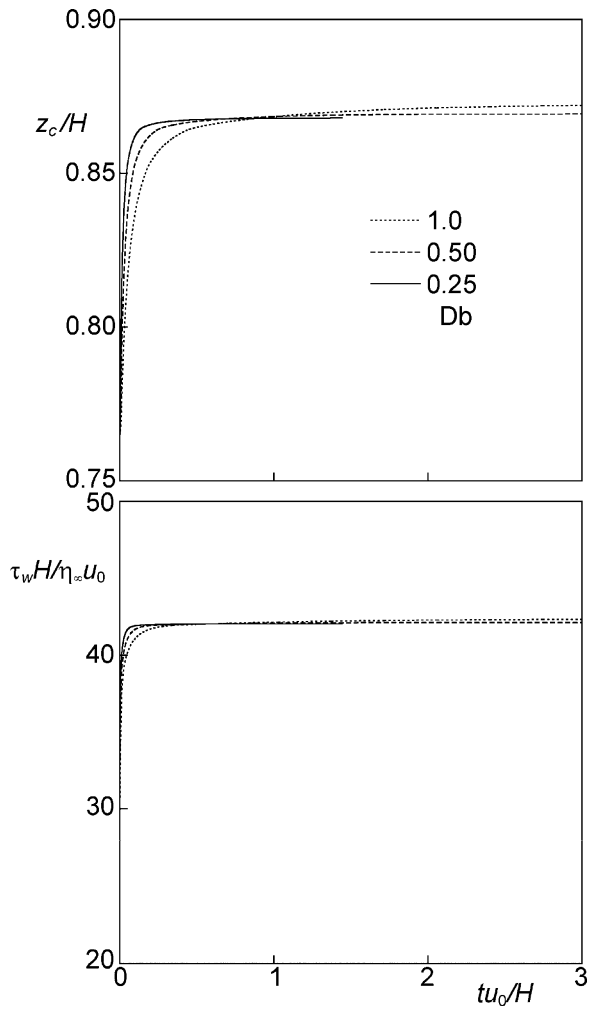

Fig. 7. Transient behavior of LDC flow after switching (at $t = 0$) from Newtonian to thixotropic liquid for three values of Db. Upper panel: vertical position of the vortex center z_c; lower panel: shear stress at the moving plate τ_w. Re = 0.5, Bn = 10, $\alpha + 1 = 250$.

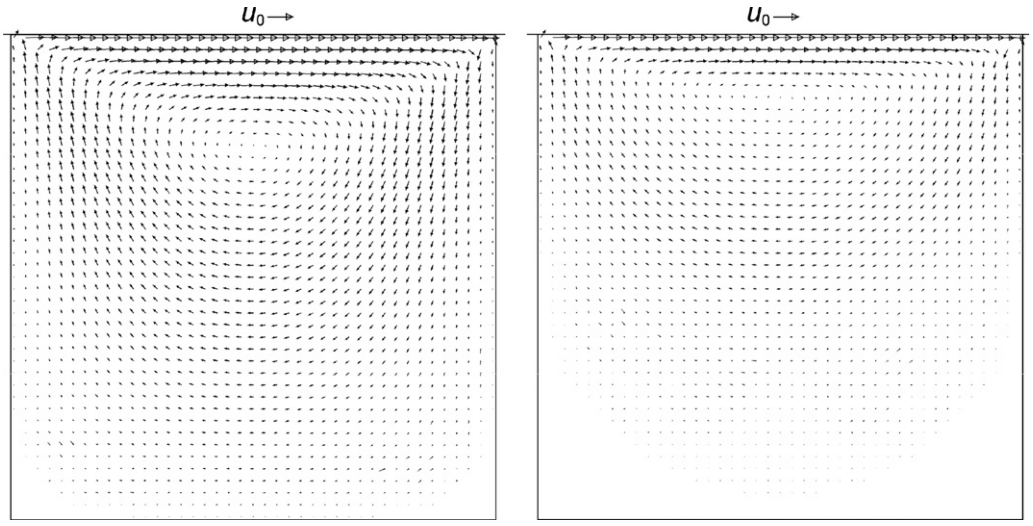

Fig. 6. Steady-state LDC flow in terms of velocity vectors. Left: Newtonian liquid, Re = 0.5. Right: thixotropic liquid, Re = 0.5, Bn = 10, Db = 0.25, $\alpha + 1 = 250$.

Table 1
Steady-state vortex core position as a function of Db. Re = 0.5, Bn = 10, $\alpha + 1 = 250$.

Db	$z_{c,\text{steady}}/H$
0	0.867
0.25	0.868
0.5	0.869
1.0	0.872
2.0	0.876

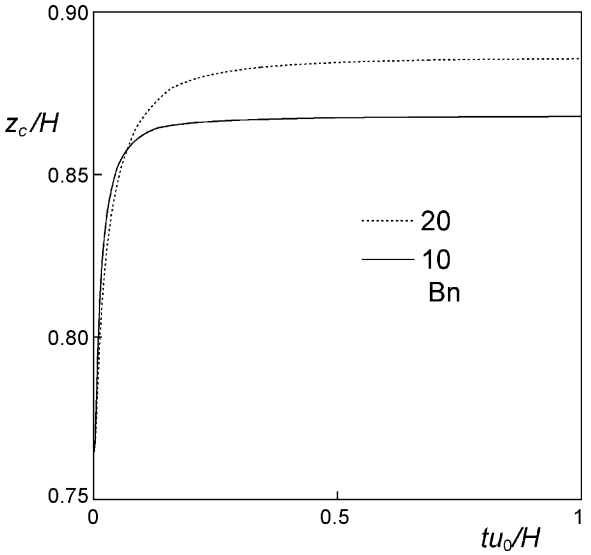

Fig. 8. Vertical position of the vortex center z_c as a function of the time after switching on thixotropic rheology; effect of the Bingham number Bn. The other dimensionless numbers were kept constant: Re = 0.5, Db = 0.25, $\alpha + 1 = 250$.

moving wall much less active, essentially limiting the flow to a small volume close to the moving wall.

In Fig. 7 we compare cases with different Deborah number (and for the rest the same parameters) in terms of the flow's response to switching on thixotropy. The higher Db, the larger the liquid's time scale and the slower the flow responds to the changed rheology. A less obvious observation is that also the steady state is a function of Db. There are slight but significant differences between the steady-state solutions at different Deborah numbers, e.g. in

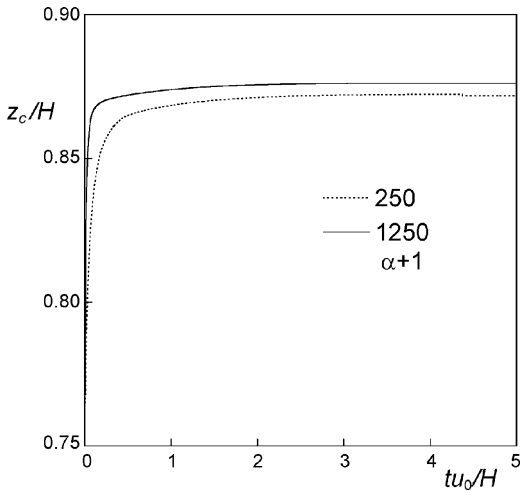

Fig. 9. Vertical position of the vortex center z_c as a function of the time after switching on thixotropic rheology; effect of the viscosity ratio $\alpha + 1$. The other dimensionless numbers were kept constant: Re = 0.5, Db = 0.25, Bn = 10.

the steady-state z-component of the vortex center position; the higher Db, the closer the vortex core gets to the moving lid (also see Table 1). The dependence of the steady flow on the liquid's time scales can be appreciated when inspecting the transport equation for the network parameter (Eq. (1)). In steady state $\partial\lambda/\partial t = 0$. However, the liquid time scales still interfere with the flow time scales (e.g. the circulation time in the cavity). The steady-state version of Eq. (1) clearly shows the coupling between velocity field and the time-dependent rheology parameters.

In Fig. 7 it is also worthwhile observing that the vortex core position is a more critical parameter for assessing steady state than the wall shear stress. The latter much quicker stabilizes and is apparently not very sensitive to (subtle) evolutions in the flow in the cavity.

As is known from earlier numerical work [24,25], increasing the Bingham number brings the vortex core closer to the moving lid. We also observe this, see Fig. 8. An increased Bingham number also gives rise to a slower response. This can be understood when the set of dimensionless numbers defining the flow (Re, Bn, Db, and α) and the way they are expressed in the primary parameters is

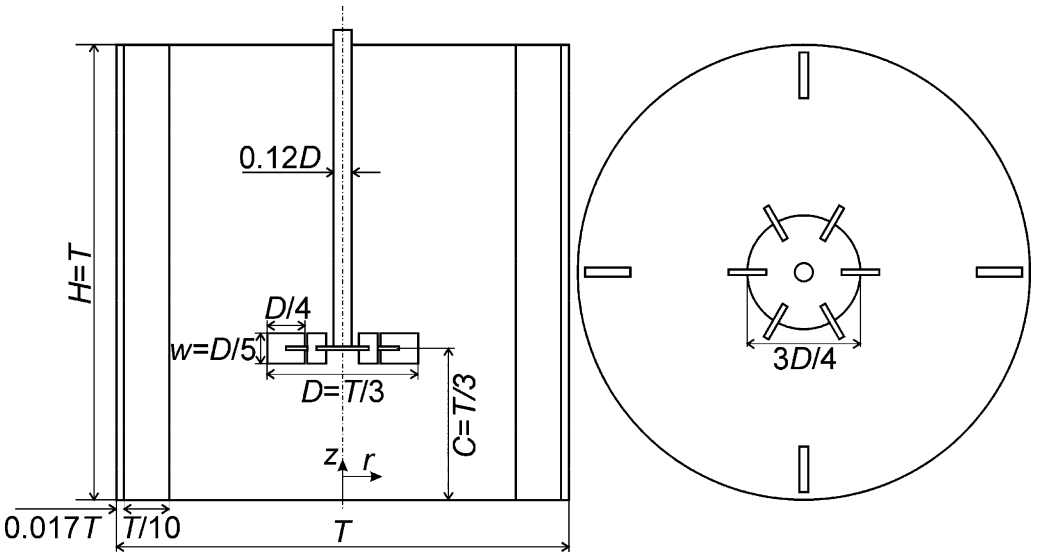

Fig. 10. Stirred tank geometry and (r,z) coordinate system. Left: side view, right: top view. The vessel content is covered with a lid (no-slip wall). The thickness of the impeller blades and disk amount to $0.035D$, the thickness of the baffles to $0.02T$.

considered. The only way to vary Bn and keeping the rest of the dimensionless numbers constant (as we do in Fig. 8) is by reducing k_1. Reducing k_1 implies reducing (in an absolute sense) the term $-k_1\dot{\gamma}\lambda$ in the network parameter transport equation which impacts the rate-of-change of λ making the flow evolution slower.

Finally, in Fig. 9 we show how the viscosity ratio α influences the dynamics of switching to a thixotropic liquid. Again both the steady state and the evolution of the flow are impacted. A higher value of α makes the regions further away from the moving lid (even) less active, driving the vortex center more towards the lid. In terms of flow dynamics, Fig. 9 quite clearly shows the occurrence of two time scales. A "fast" one relates to the initially steep rise of z_c, i.e. the z-location of the vortex core. At some stage in time (at about $tu_0/H = 0.5$ if $\alpha + 1 = 250$; at $tu_0/H = 0.15$ if $\alpha + 1 = 1250$) a slower time scale takes over. The slower time scale is (roughly) the same for the two cases shown in the figure and can be traced back to $1/k_2$ (since Db = 1, $1/k_2 = H/u_0$) being the same for both cases considered in Fig. 9. Next to the $1/k_2$ time scale, Eq. (1) contains a second time scale related to k_1. The faster time we now try to interpret in terms of the $-k_1\dot{\gamma}\lambda$ term in Eq. (1): a higher α at the same Bingham and Deborah number (and the same Re) implies a higher k_1. The time scale $1/k_1\dot{\gamma}$ we may write as $1/k_1\dot{\gamma} = H/k_1Cu_0 = \mathrm{Bn}/C\alpha k_2$ where the shear rate is written as some effective shear rate that scales with u_0/H: $\dot{\gamma} = Cu_0/H$. Then, with Bn = 10, the fast time scale $1/k_1\dot{\gamma}$ relates to the slow time scale $1/k_2$ according to $1/k_1\dot{\gamma} = (10/C\alpha)(1/k_2)$. If we (quite speculatively) set to $C = 0.25$, the coefficient $10/C\alpha$ is 0.16 for $\alpha + 1 = 250$, and 0.03 for $\alpha + 1 = 1250$. If one realizes that the 0.16 and 0.03 actually are dimensionless e^{-1} decay times, the observed values of 0.5 and 0.15 for $\alpha + 1 = 250$ and $\alpha + 1 = 1250$ respectively can be tentatively traced back to the $-k_1\dot{\gamma}\lambda$ term in the λ transport equation.

The intermediate conclusions from the benchmark results are that thixotropy effects are indeed accurately resolved with the simulation procedure and that interpretation of results quickly gets more intricate with increasing flow complexity (from simple shear, to plane Poiseuille, to LDC flow).

5. Thixotropic liquids in mixing tanks

We now turn to flows of thixotropic liquids in mixing tanks. The geometry of the mixing tank and the impeller are given in Fig. 10, along with a definition of the coordinate system. The impeller, a Rushton turbine, is a de facto standard impeller in mixing research and therefore allows for comparison with a large body of numerical and experimental data regarding Newtonian and (to a lesser extent) non-Newtonian liquids. It consists of a round disk with six flat blades mounted on its perimeter. The tank has baffles at its perimeter that enhance mixing as they prevent the liquid from rotating largely as a solid body under the influence of the revolving impeller. In this standard configuration all tank and impeller

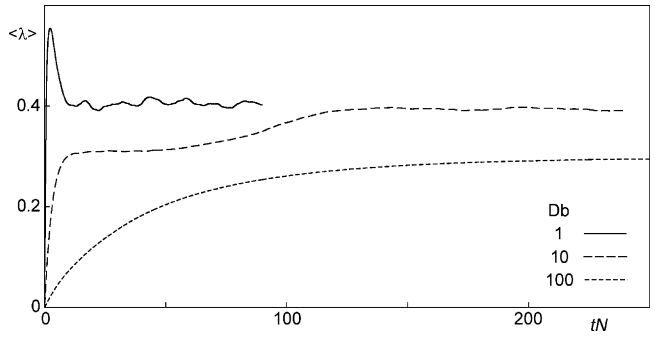

Fig. 11. Time series of the tank-averaged λ for three values of Db when starting up from a zero flow, and zero λ field.

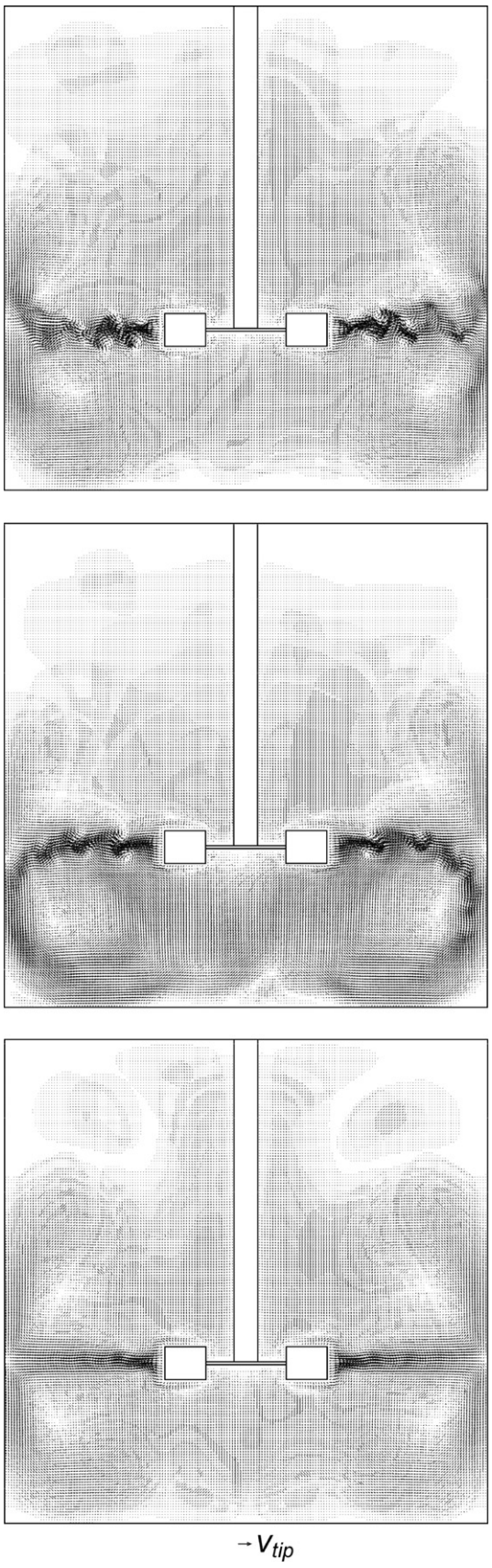

Fig. 12. Velocity vectors in a vertical cross-section midway between baffles of single realizations of flows with three different Deborah numbers (from top to bottom: Db = 1, 10, and 100). The snapshots were taken after each flow system reached quasi steady state.

dimensions can be derived from the tank diameter T (see Fig. 10), e.g. the impeller diameter $D = T/3$.

In mixing of Newtonian liquids in stirred tanks the Reynolds number is traditionally defined as $\mathrm{Re} = \rho N D^2/\eta$ with N the impeller speed (in rev/s). In analogy we here define the Reynolds number as $\mathrm{Re}_\infty = \rho N D^2/\eta_\infty$. The additional three dimensionless numbers if thixotropic liquid mixing is being considered are chosen in analogy with the lid-driven cavity benchmark: $\mathrm{Db} = N/k_2$, $\mathrm{Bn} = \alpha(k_2/k_1)(1/N)$, and α.

The mixing tank flow cases we are interested in would be mildly turbulent if the liquid is Newtonian with viscosity η_∞ ($\mathrm{Re}_\infty = O(10^4)$), and laminar if the viscosity is $\eta_\infty(1+\alpha)$ ($\mathrm{Re}_\infty/(1+\alpha) = O(10^2)$). As for Re_∞, we do not want to go beyond 10^4 in order to keep in a Reynolds number range amenable to direct numerical simulations (DNS) and avoid the use of turbulence modeling.

The tanks to be simulated are of lab-scale size with a tank volume of typically 10 l. A 10-l tank with geometrical layout as given in Fig. 10 has a diameter $T = 0.234$ m. The impeller diameter $D = T/3 = 0.078$ m. With a liquid having $\eta_\infty = 10^{-2}$ Pa s and $\rho = 10^3$ kg/m^3 we generate mildly turbulent flow if the impeller spins with $N = 10$ rev/s: $\mathrm{Re}_\infty = 6{\cdot}10^3$. Commonly used thixotropic liquids have time constants in the range of 0.1–10 s (see e.g. Dullaert and Mewis [26]), so that the Deborah numbers fall in the range 1 to 100. To end up with laminar flow if the network would be fully developed ($\lambda = 1$ everywhere) we set $\alpha + 1 = 100$. Furthermore, we set the Bingham number to the fixed value of $\mathrm{Bn} = 100$. Under the conditions sketched above (tank size, impeller speed, other liquid properties) this would correspond to a (pseudo) yield stress of $\tau_Y = 10$ N/m^2. To summarize the physical settings of the simulations: three of the four dimensionless numbers are fixed: $\mathrm{Re}_\infty = 6{\cdot}10^3$, $\mathrm{Bn} = 100$, $\alpha + 1 = 100$. The Deborah number we vary by considering three values: Db = 1, 10, 100.

As mentioned above, the liquid flow dynamics was resolved using the lattice-Boltzmann method. In its basic implementation (as used in this study) the method applies a uniform, cubic grid. The spatial resolution of the grid was such that the tank diameter T equals 180 grid spacings Δ. The time step is such that the impeller revolves once in 2000 time steps. The rotation of the impeller in the static grid is represented by an immersed boundary technique. The spatial resolution of $\Delta = T/180$ is sufficient to fairly accurately capture the main features of (Rushton) stirred tank flow. Higher resolutions would have been feasible and to a certain extent beneficial [27]. Given the explorative nature of this study, the long runs (in terms of numbers of impeller revolutions) that we expect, and the desire to do parameter variation it was decided to apply this relatively modest spatial resolution.

As the default situation, the simulations were started with a zero liquid velocity field and a uniform network parameter $\lambda = 0$ (no network). Our primary interests are in how the flow develops towards a (quasi) steady state, what flow structures can be observed in (quasi) steady state, and what the influence of the Deborah number is on all this.

5.1. Flow development

In Fig. 11 we show the development of the tank-average structure parameter $\langle\lambda\rangle$ after starting from a zero flow, and zero λ field. Clearly, the higher Db the slower the network develops. In addition, the path along which the three cases approach quasi steady state is very different. At Db = 1 the network builds up quicker than the flow that starts around the impeller can penetrate the bulk of the tank. This results in an initial overshoot of $\langle\lambda\rangle$ with λ quickly increasing in the still quiescent parts of the tank. In a later stage the flow erodes the networked zones in the tank and $\langle\lambda\rangle$ decreases again after which a quasi steady state is reached. For Db = 10 the development towards steady state has a relatively fast stage (with a time scale associated to it of the order of k_2^{-1}) and a slow stage taking of the order of 150 impeller revolutions. At the highest Db (Db = 100) the system very gradually goes towards steady state.

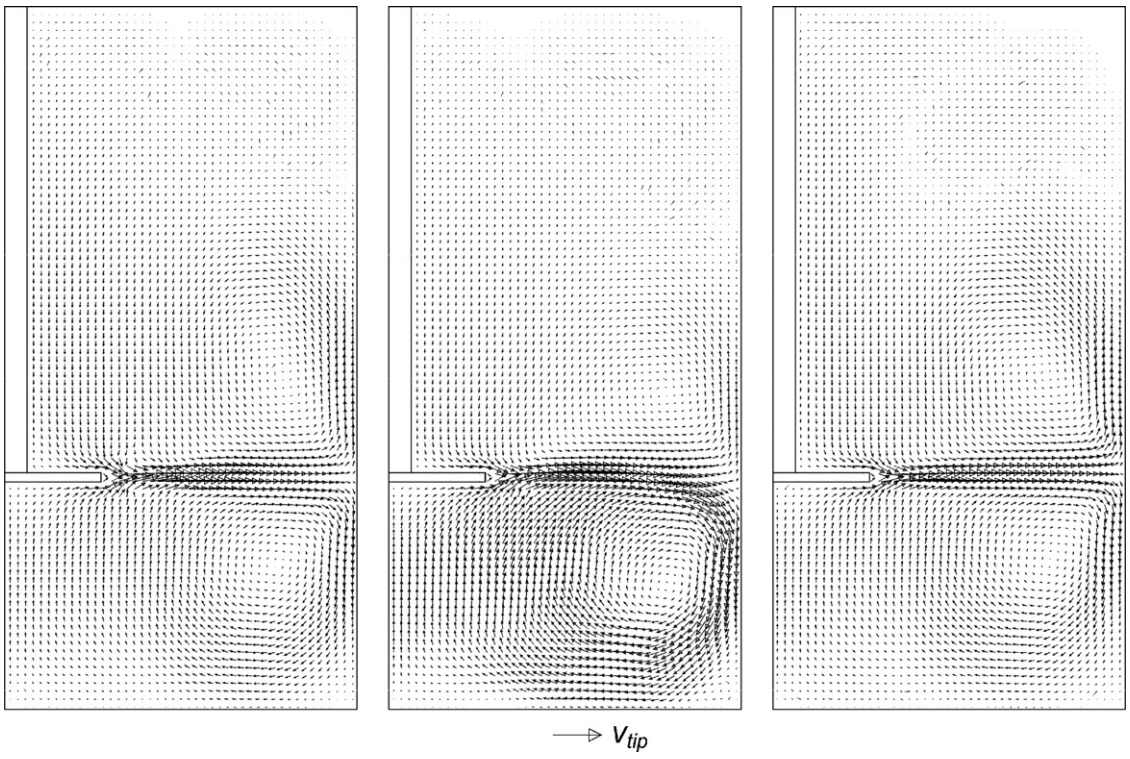

Fig. 13. Time averaged velocity field in the vertical plane midway between baffles. Averages taken in quasi steady state over at least 20 impeller revolutions. From left to right: Db = 1, 10, and 100.

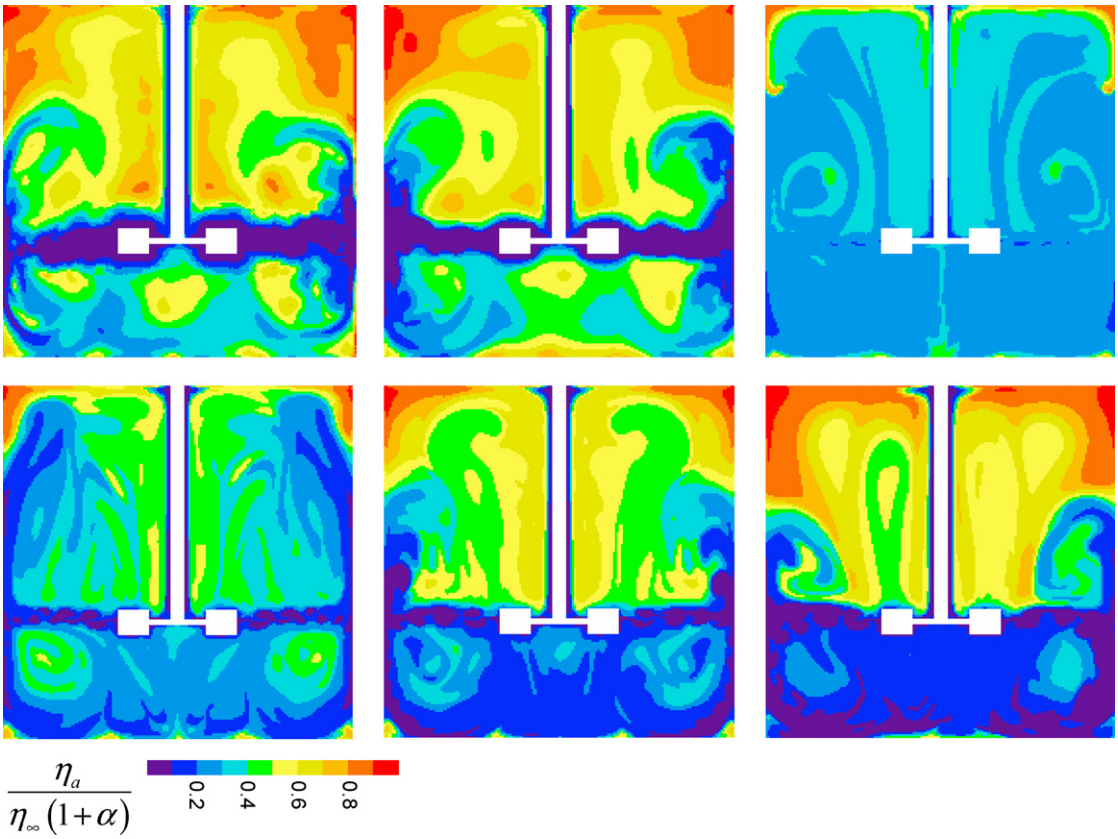

Fig. 14. Snapshots of the apparent viscosity η_a relative to $\eta_\infty(\alpha+1)$ in a vertical cross-section through the tank. Top row from left to right: Db = 0 at $tN = 60$, Db = 1 at $tN = 60$, Db = 100 at $tN = 250$. Bottom row: Db = 10 and (from left to right) $tN = 50, 100, 210$.

Before looking into this development more closely, e.g. in terms of the spatial distribution of the network parameter in the tank, first the overall structure of the flow under quasi steady conditions is examined. In Fig. 12 snapshots (i.e. single realizations) of vertical cross-sections through the flows in terms of velocity vectors are displayed; all three snapshots were taken at moments the flow had become quasi steady, as identified via Fig. 11. As we already saw for lid driven cavity flow, liquids that have the same steady-state rheology and are only different in terms of their network time scale develop different flow structures, not only in transitional (unsteady) stages, also in quasi steady state. At Db = 1 the impeller outstream has some level of turbulence. The circulation pattern, however, extends only into part of the tank, with large inactive zones specifically in the upper part of the tank. The result of the Db = 10 simulation is peculiar, with a circulation stream only present in the region below the impeller, and an inactive region above. The route towards this situation will be discussed in more detail below. The case with Db = 100 is again very different. The trailing vortex system in the impeller outstream so typical for the flow driven by a Rushton turbine [2] has completely disappeared here; the flow clearly being dominated by viscous forces everywhere.

To make clear that the snapshots of Fig. 12 are representative for the steady state at each of the Deborah numbers, time-averages vectors fields collected during (at least) 20 impeller revolutions in steady state are shown in Fig. 13. In terms of the average flow, the distinction between the Db = 1 and Db = 100 case has largely disappeared since the trailing vortex structures emerging from the impeller and moving in radial direction towards the tank wall get averaged out.

The above sketched development and eventual stages can be better understood by monitoring the way the network parameter λ, or (since they are one-on-one related via Eq. (2)) the apparent viscosity gets distributed in the mixing tank. If Db = 100, the liquid's time scales are much longer than almost all relevant flow time scales. In other words, the mixing is very fast compared to the build-up and breakdown of the network which leads to a fairly uniform (well-mixed) distribution of the apparent viscosity, see Fig. 14 (upper right panel). This situation is comparable to a very slow chemical reaction taking place in a vigorously mixed tank. Under such conditions the tank can be considered ideally mixed with approximately uniformly distributed concentrations. At the specific settings of this simulation, the level of the apparent viscosity ultimately gets of the order of $20\eta_\infty$ throughout the tank which corresponds to a Reynolds number of $\mathrm{Re}_a = \rho N D^2/\eta_a \approx 300$, indicating laminar flow indeed.

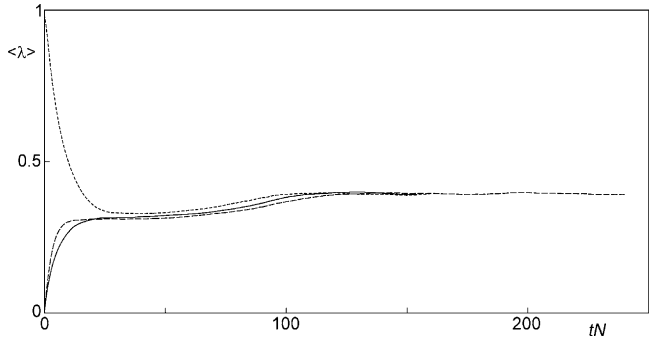

Fig. 15. Time series of the tank-averaged λ for Db = 10, with three different initial conditions. Solid line: fully developed Newtonian flow with Re = 6000 and $\lambda = 0$; long-dashed line: zero flow and $\lambda = 0$ (same as Fig. 11); short dashed line: zero flow and $\lambda = 1$.

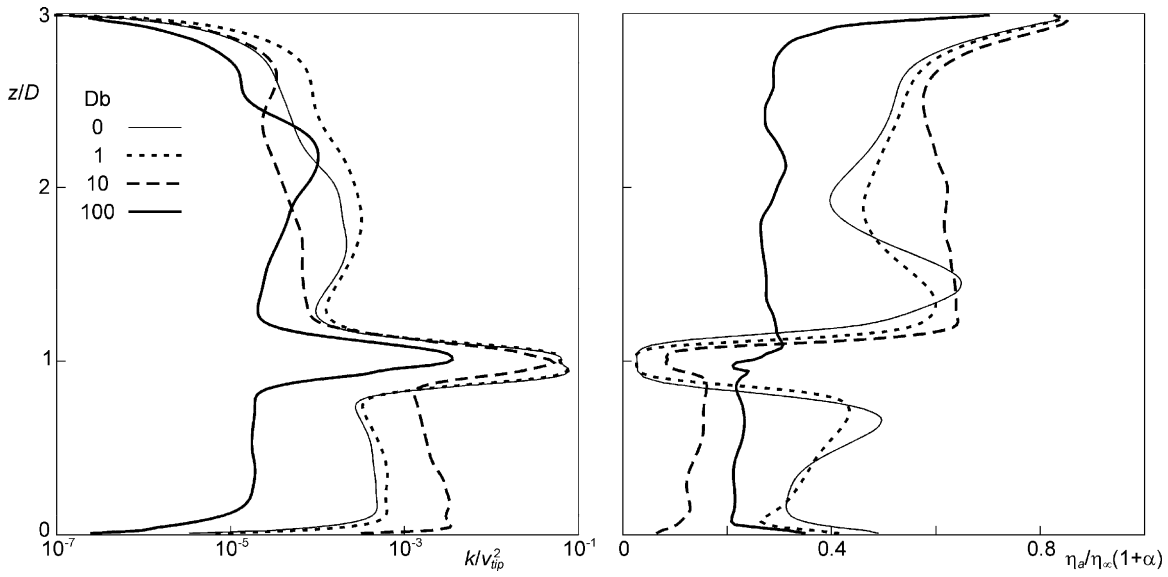

Fig. 16. Vertical profiles at a radial position of $r = T/4$ of the time-average kinetic energy k, and the apparent viscosity η_a for the various Deborah numbers.

The Db = 1 case gives rise to a very inhomogeneous distribution of the apparent viscosity in the tank, with low levels close to the impeller and in the stream emerging from the impeller where the network is destroyed continuously due to liquid deformation, and high levels in the dead zones in (for instance) the upper corners (see Fig. 14, upper center panel). This distribution creates active and relatively inactive regions in the tank. For comparison we also show in Fig. 14 (upper left panel) a distribution of the apparent viscosity if Db = 0, which we get if instead of a thixotropic liquid we have a time independent liquid with the steady-state rheology of Eq. (4). The apparent viscosity distributions with Db = 1 is very similar to the one with Db = 0 indicating that for Db = 1 (and the rest of the current conditions: flow geometry, other dimensionless numbers) the time dependence of the liquid is not strongly felt.

The most intriguing case is the one with Db = 10. Some 40 revolutions after start-up the system tends to steady state. However, beyond 50 revolutions $\langle\lambda\rangle$ starts slowly but systematically increasing again until it levels off after 150 revolutions after start-up. This behavior is quite insensitive for the initial conditions as can be appreciated from Fig. 15: in addition to the simulation starting from zero flow and zero network, also simulations starting from zero flow and fully developed network, and fully developed Newtonian flow (with viscosity η_∞) were preformed, showing similar long-time behavior. What happens in the slow part of the flow's development (between 50 and 150 revolutions) is a slow build-up of the network in the upper part of the tank which gradually pushes the impeller stream down until the liquids only recirculates underneath the impeller, see Fig. 14 (lower three panels). This is the steady state as also identified in Figs. 12 and 13.

5.2. Quasi steady-state flow

In order to compare the different stirred tank cases in a more quantitative manner, profiles of the kinetic energy contained in the velocity fluctuations u_i' (turbulent and deterministic due to impeller rotation) $k = (1/2)u_i'u_i'$, and time-averaged apparent viscosity have been determined, see Fig. 16. A few qualitative observations made above are confirmed by these profiles. In the first place we note the small difference between the flow at Db = 1 and Db = 0. Both the viscosity and kinetic energy profiles show strong resemblance. The conclusion is that a thixotropic liquid with a network time scale of the same order of magnitude as the time needed for one impeller revolutions effectively behaves as a time-independent liquid. In the second place, the profiles show that in all cases considered velocity fluctuations (as expressed in kinetic energy) are confined to the impeller region, and the liquid stream emerging from the impeller. In the rest of the tank fluctuation levels are negligible (note the logarithmic scale of the k-profiles). In the third place there is the sharp division between an active (underneath the impeller) and an inactive volume if Db = 10.

6. Summary and outlook

In this paper a procedure for flow simulations involving viscous thixotropic liquids has been outlined. Thixotropy enters via a scalar quantity λ that represents the level of integrity of a structural network in the liquid. A highly developed network (λ close to 1) implies high viscosity, λ close to zero implies low viscosity. The network can be given a characteristic time to build-up, and gets disintegrated due to fluid deformation. The simulation procedure is based on the lattice-Boltzmann method for solving the flow equations, and an explicit finite volume method for solving the transport equation in λ. It is numerically very efficient and therefore allows for highly resolved simulations that we use to study flows in complexly shaped confinements at relatively high Reynolds numbers (transitional and turbulent flows).

The simulation method has been verified by applying it to three benchmark cases: simple shear flow, planar Poiseuille flow, and lid-driven cavity flow. In the former two cases very good agreement between numerical results and (semi-) analytical solutions has been obtained. The lid-driven cavity case highlights the interesting interactions between flow time scales (circulation time in this case), and time scales related to thixotropy; also in steady flows the time scale of the liquid matters.

The full potential of the algorithms has been utilized by performing direct numerical simulations of the flow in a mixing tank in the laminar and transitional regime with a focus of the role of the Deborah number (the ratio of the liquid time scale and impeller revolution period). A high Deborah number (Db = 100 in this paper) results in an almost uniform distribution of the network parameter in the mixing tank. If Db = 1, the thixotropic liquid effectively behaves as a time-independent liquid and develops (with the steady-state rheology as chosen here) flow structures reminiscent of Bingham liquids in agitated tanks. The case with Db = 10 shows

peculiar behavior. Its transient has two time scales of which the faster can be directly traced back to the time scale of the liquid. The slower has to be due to an intricate interaction between flow conditions and liquid properties. The global quasi-steady flow structure shows a sharp distinction between an active part underneath the impeller, and an inactive part above. In practical situations such behavior would be highly undesirable since it leaves a large part of the tank's volume (and mixing capacity) unused. The simulation results call for experimental work on similar flow systems and liquids.

The simulations presented here were run in sequential mode. The procedure, however, can be trivially extended to allow for computationally very efficient parallel simulation so that higher resolution and/or computation speed can be achieved.

The work presented is mainly motivated by the challenges posted by processing waste streams in oil sands processing (tailings). We plan to perform simulations of dense solid–liquid mixtures with direct resolution of the solid–liquid interfaces, as to predict mobility of solid particles in thixotropic liquids. The lattice-Boltzmann method allows for such simulations as has been demonstrated for solids in Newtonian liquids [28]. The results with thixotropic liquids could provide useful insights in the consistency of tailings which is important for land reclamation at the end of the oil sands production cycle.

References

[1] J. Masliyah, Z.J. Zhou, Z. Xu, J. Czarnecki, H. Hamza, Understanding water-based bitumen extraction from Athabasca oil sands, Can. J. Chem. Eng. 82 (2004) 628.
[2] J. Derksen, H.E.A. Van den Akker, Large-eddy simulations on the flow driven by a Rushton turbine, AIChE J. 45 (1999) 209.
[3] H. Hartmann, J.J. Derksen, C. Montavon, J. Pearson, I.S. Hamill, H.E.A. van den Akker, Assessment of large eddy and RANS stirred tank simulations by means of LDA, Chem. Eng. Sc. 59 (2004) 2419.
[4] D.Z. Yu, R.W. Mei, L.S. Luo, W. Shyy, Viscous flow computations with the method of lattice Boltzmann equation, Progr. Aerosp. Sci. 39 (2003) 329.
[5] S. Chen, G.D. Doolen, Lattice Boltzmann method for fluid flows, Annu. Rev. Fluid Mech. 30 (1998) 329.
[6] S. Succi, The Lattice Boltzmann Equation for Fluid Dynamics and Beyond, Clarondon Press, Oxford, 2001.
[7] J. Mewis, Thixotropy—a general review, J. Non-Newt. Fluid Mech. 6 (1997) 1.
[8] A. Mujumdar, A.N. Beris, A.B. Metzner, Transient phenomena in thixotropic systems, J. Non-Newt. Fluid Mech. 102 (2002) 157.
[9] B.T. Storey, E.W. Merrill, The rheology of aqueous solution of amylose and amylopectin with reference to molecular configuration and intermolecular association, J. Polym. Sci. 33 (1958) 361.
[10] F. Moore, The rheology of ceramic slips and bodies, Trans. Br. Ceram. Soc. 58 (1959) 470.
[11] T. Ferroir, H.T. Huynh, X. Chateau, P. Coussot, Motion of a solid object through a pasty (thixotropic) fluid, Phys. Fluids 16 (2004) 594.
[12] C.R. Beverly, R.I. Tanner, Numerical analysis of extrudate swell in viscoelastic materials with yield stress, J. Rheol. 33 (1989) 989.
[13] U. Frisch, B. Hasslacher, Y. Pomeau, Lattice-gas automata for the Navier–Stokes equation, Phys. Rev. Lett. 56 (1986) 1505.
[14] M.C. Sukop, D.T. Thorne Jr., Lattice Boltzmann Modeling: An Introduction for Geoscientists and Engineers, Springer, Berlin, 2006.
[15] M. Yoshino, Y. Hotta, T. Hirozane, M. Endo, A numerical method for incompressible non-Newtonian fluid flows based on the lattice Boltzmann method, J. Non-Newt. Fluid Mech. 147 (2007) 69.
[16] A. Vikhansky, Lattice-Boltzmann method for yield-stress liquids, J. Non-Newt. Fluid Mech. 155 (2008) 95.
[17] J.J. Derksen, Solid particle mobility in agitated Bingham liquids, Ind. Eng. Chem. Res. 48 (2009) 2266.
[18] J.A. Somers, Direct simulation of fluid flow with cellular automata and the lattice-Boltzmann equation, Appl. Sci. Res. 51 (1993) 127.
[19] D. Goldstein, R. Handler, L. Sirovich, Modeling a no-slip flow boundary with an external force field, J. Comp. Phys. 105 (1993) 354.
[20] J.J. Derksen, Simulations of confined turbulent vortex flow, Comput. Fluids 34 (2005) 283.
[21] J.G.M. Eggels, J.A. Somers, Numerical simulation of free convective flow using the lattice-Boltzmann scheme, Int. J. Heat Fluid Flow 16 (1995) 357.
[22] J.J. Derksen, Scalar mixing by granular particles, AIChE J. 54 (2008) 1741.
[23] P.K. Sweby, High resolution schemes using flux limiters for hyperbolic conservation laws, SIAM J. Numer. Anal. 21 (1984) 995.
[24] E. Mitsoulis, Th. Zisis, Flow of Bingham plastics in a lid-driven square cavity, J. Non-Newt. Fluid Mech. 101 (2001) 173.
[25] Z. Yu, A. Wachs, A fictious domain method for dynamic simulation of particle sedimentation in Bingham fluids, J. Non-Newt. Fluid Mech. 145 (2007) 78.
[26] K. Dullaert, J. Mewis, Thixotropy: build-up and breakdown curves during flow, J. Rheol. 49 (2005) 1213.
[27] J. Derksen, Assessment of large eddy simulations for agitated flow, Trans. IChemE 79 (2001) 824.
[28] J.J. Derksen, S. Sundaresan, Direct numerical simulations of dense suspensions: wave instabilities in liquid-fluidized beds, J. Fluid Mech. 587 (2007) 303.